Mechanics of Materials 59 (2013) 110–125

Contents lists available at SciVerse ScienceDirect

Mechanics of Materials

journal homepage: www.elsevier.com/locate/mechmat

Fields produced by three-dimensional dislocation loops in anisotropic magneto-electro-elastic materials

Xueli Han [a,*], Ernie Pan [b,c]

[a] Department of Mechanics, School of Aerospace, Beijing Institute of Technology, Beijing 100081, China
[b] Computer Modeling and Simulation Group, University of Akron, Akron, OH 44324-3905, USA
[c] School of Mechanical Engineering, Zhengzhou University, Zhengzhou 450001, China

ARTICLE INFO

Article history:
Received 2 March 2012
Received in revised form 10 August 2012
Available online 18 September 2012

Keywords:
Dislocation loop
Three-dimensional
Magneto-electro-elastic materials
Anisotropy
Parametric dislocation

ABSTRACT

In this article, we analyze the coupled elastic, electric and magnetic fields produced by an arbitrary three-dimensional dislocation loop in general anisotropic magneto-electro-elastic materials. We first extend the anisotropic elastic formulae of dislocations to the corresponding magneto-electro-elastic material system, including a general line-integration solution and the solution of a straight-line segment of dislocation. We then develop a new line-integral solution for the extended displacement field as well as the extended stress field. Furthermore, we derive analytical expressions for some useful parametric dislocation curves, such as the elliptic arc and straight line. Our solutions contain the piezoelectric, piezomagnetic, and purely anisotropic elastic solutions as special cases. As numerical examples, the fields produced by elliptic, hexagonal and cardioid shape dislocation loops in both piezoelectric crystals and magneto-electro-elastic materials are calculated. The efficiency and accuracy of different integral solutions of dislocation loops are compared and discussed. More important, the coupling magneto-electro-elastic effect is illustrated. It is shown that, due to the coupling among the elastic, electric and magnetic fields, an elastic dislocation, an electric potential discontinuity, or a magnetic potential discontinuity can induce all the elastic, electric and magnetic fields and that the coupling effect could be very strong near the dislocation loop line.

1. Introduction

The piezoelectric material, which possesses the coupling effect between mechanical and electric fields, is now being widely applied to different engineering technologies. This stimulates various theoretical studies on such coupling materials. One of the studies is on the dislocations and their movements since they play an important role in the physical behaviors of materials. While fracture mechanics problems in piezoelectric materials have been well investigated for both two-dimensional and three-dimensional problems (e.g., Suo et al., 1992; Zhang et al., 2002), the corresponding dislocation problems were mostly investigated for two-dimensional domains only (e.g., Pak, 1990; Liu et al., 1999; Chen et al., 2004; Wang and Sudak, 2007) where the dislocations were taken to be infinite straight line. In reality, however, dislocations usually form three-dimensional loops which are more difficult to analyze. Although Minagawa and Shintani (1985), Minagawa (2003) studied the stress and electric fields produced by dislocation loops, the procedure and solution were complicated and only the elastic displacement dislocation was considered. Nowacki and Alshits (2007) extended the dislocation-field expression to piezoelectricity but no numerical example was given. Dislocations in piezoelectric and magneto-electro-elastic (MEE) materials could show some interesting features and deserve further investigation. For instance, due to the coupling between

* Corresponding author.
E-mail addresses: hanxl@bit.edu.cn (X. Han), pan2@uakron.edu (E. Pan).

0167-6636/$ - see front matter © 2012 Elsevier Ltd. All rights reserved.
http://dx.doi.org/10.1016/j.mechmat.2012.09.001

the mechanical and electric fields, a moving dislocation in piezoelectric crystal could induce certain interesting coupling features (Soh et al., 2005). Further due to the coupling, the dislocation mobility (Li and Gupta, 2004) and energetics of a partial dislocation (Belabbas et al., 2006) could be different than those in the purely elastic domain. Other important and potential applications of the dislocation solution in piezoelectric materials include the induced polarization feature in such materials (Shi et al., 1999). Since most technically important materials would be also ferroelectric, the dislocation solution could be further applied to study the dislocation-induced polarization variation and distributions (Zheng et al., 2006), their effect on ferroelectric phase stability, domain morphology (Hu et al., 2003) and possible degradation of ferroelectric properties (Alpay et al., 2004). Composites made of piezoelectric/piezomagnetic materials exhibit magnetoelectric coupling effect that is not present in the single-phase piezoelectric or piezomagnetic material. In the past decade, much attention has been paid to predict the effective properties of MEE composites according to the theories of micromechanics. But for dislocation problems in MEE, relatively little work has been done. Until now, only one-dimensional dislocations in such coupling materials were studied (Hao and Liu, 2006; Ma and Lee, 2007; Lee and Ma, 2010).

Motivated by the important applications of the MEE material and the potential influence of dislocations on such a material, we derive, in this paper, the extended stress fields induced by the extended dislocation loops by utilizing the extended Green's functions and their derivatives in MEE materials. We present three forms of the solutions: a line integral form for smooth dislocation loops which can be evaluated by a standard numerical integration method, an analytical expression which is for the loops made of piecewise straight lines, and the analytical solution for some parametric curve loops, such as elliptic arcs. Numerical examples are presented for elliptic, hexagonal and cardioid dislocation loops in piezoelectric materials GaAs and AlN and in MEE composites made of $BaTiO_3$–$CoFe_2O_4$. Our results show clearly the important coupling features among mechanical, electric and magnetic fields.

2. Basic equations

With the extended notation (Barnett and Lothe, 1975), the equilibrium equations (including the electric and magnetic balance equations) and the constitutive relations for the coupled MEE media can be expressed as (Pan, 2002):

$$\sigma_{ij,i} + f_J = 0, \quad \sigma_{iJ} = C_{iJKl}\gamma_{Kl} \tag{1}$$

The summation over repeated lowercase (uppercase) subscripts is from 1 to 3 (1–5), and a subscript comma denotes the partial differentiation with respect to the coordinates. The extended displacement, body force, strain and stresses are defined as

$$u_I = \begin{cases} u_i, & I = i = 1,2,3 \\ \phi, & I = 4 \\ \psi, & I = 5 \end{cases} \tag{2a}$$

$$f_J = \begin{cases} f_j, & J = j = 1,2,3 \\ -f_e, & J = 4 \\ -f_m, & J = 5 \end{cases} \tag{2b}$$

$$\gamma_{Ij} = \begin{cases} \gamma_{ij} = 0.5(u_{i,j} + u_{j,i}), & I = i = 1,2,3 \\ -E_j = \phi_{,j}, & I = 4 \\ -H_j = \psi_{,j}, & I = 5 \end{cases} \tag{2c}$$

$$\sigma_{iJ} = \begin{cases} \sigma_{ij}, & J = j = 1,2,3 \\ D_i, & J = 4 \\ B_i, & J = 5 \end{cases} \tag{2d}$$

and the extended elastic coefficient matrix has the following components

$$C_{iJKl} = \begin{cases} C_{ijkl}, & J,K = j,k = 1,2,3 \\ e_{lij}, & J = j = 1,2,3;\ K = 4 \\ e_{ikl}, & J = 4;\ K = k = 1,2,3 \\ q_{lij}, & J = j = 1,2,3;\ K = 5 \\ q_{ikl}, & J = 5;\ K = k = 1,2,3 \\ -\alpha_{il}, & J = 4;\ K = 5 \text{ or } J = 5; K = 4 \\ -\varepsilon_{il}, & J = K = 4 \\ -\mu_{il}, & J = K = 5 \end{cases} \tag{3}$$

In Eqs. (1), (2a), (2b), (2c), (2d), (3), u_i, ϕ and ψ are the elastic displacement, electric potential and magnetic potential; f_i, f_e and f_m are the body force, electric charge and electric current; γ_{ij}, E_i and H_i are the strain, electric field and magnetic field; σ_{ij}, D_i and B_i are the stress, electric displacement and magnetic induction, respectively; C_{ijlm}, ε_{ij}, and μ_{ij} are the elastic, dielectric and magnetic permeability tensors, e_{ijk}, q_{ijk} and α_{ij} are the piezoelectric, piezomagnetic, and magnetoelectric coefficients, respectively. The material constants satisfy the following symmetry relations:

$$\begin{aligned} &C_{ijkl} = C_{ijlk} = C_{jikl} = C_{klij}; \varepsilon_{ij} = \varepsilon_{ji}; \mu_{ij} = \mu_{ji} \\ &e_{kij} = e_{kji}; q_{kij} = q_{kji}; \alpha_{ij} = \alpha_{ji} \end{aligned} \tag{4}$$

It is noted that we assumed that the magnetoelectric coefficient matrix α_{ij} is symmetric and that we have

$$C_{iJKl} = C_{lKJi} \quad \text{but} \quad C_{iJKl} \neq C_{iJlK} \neq C_{JiKl} \neq C_{KliJ} \tag{5}$$

The extended Green's functions (5×5 tensor) $G_{KM}(y;\boldsymbol{x})$ are defined as the extended displacement component $u_K(\boldsymbol{x})$ at a field point $\boldsymbol{x}$ due to an extended unit point force in M-direction at the source point $\boldsymbol{y}$. They satisfy the equilibrium equation

$$[C_{iJKl}(\boldsymbol{x})G_{KM,x_l}(\boldsymbol{y};\boldsymbol{x})]_{,x_i} + \delta_{JM}\delta(\boldsymbol{y};\boldsymbol{x}) = 0 \tag{6}$$

with $f_{,x_i} = \partial f/\partial x_i$, δ_{JM} being the fifth-rank Kronecker delta, and $\delta(\boldsymbol{y};\boldsymbol{x})$ the Dirac-delta function which is zero everywhere except at point $\boldsymbol{x} = \boldsymbol{y}$. The solutions of the extended Green's functions and their derivatives are given in Appendix A.

Consider a region V in the 3D space which is bounded by the surface S. If $\boldsymbol{x}$ is inside the region, then multiplying Eq. (6) by u_J and integrating through the region, we have

$$u_M(\boldsymbol{y}) = -\int_V [C_{iJKl}(\boldsymbol{x})G_{KM,x_l}(\boldsymbol{y};\boldsymbol{x})]_{,x_i} u_J(\boldsymbol{x})dV(\boldsymbol{x}) \tag{7}$$

Making use of the divergence theorem and the equilibrium equations and constitutive relation (1), we obtain

$$u_M(\boldsymbol{y}) = \int_{\partial V} [G_{JM}(\boldsymbol{y};\boldsymbol{x})\sigma_{iJ}(\mathbf{x}) - C_{iJKl}(\boldsymbol{x})G_{KM,x_l}(\boldsymbol{y};\boldsymbol{x})u_J(\boldsymbol{x})]n_i(\boldsymbol{x})dS(\boldsymbol{x}) + \int_V G_{JM}(\boldsymbol{y};\boldsymbol{x})f_J(\boldsymbol{x})dV(\boldsymbol{x}) \tag{8}$$

With ∂V being the surface of V including all inner surfaces, and $\boldsymbol{n}$ being the unit normal to ∂V. Eq. (8) is an integral expression of the extended displacement in terms of the extended point-force Green's functions.

3. Fields produced by a dislocation loop

We now consider the elastic, electric and magnetic fields produced by an arbitrary shaped extended dislocation loop in an infinite anisotropic MEE medium. The extended dislocation loop L is defined as the boundary of a surface S where the elastic displacement has a jump $\mathbf{b}$, the electric potential a jump $\Delta\phi$, and the magnetic potential a jump $\Delta\psi$. In other words, across S, we have

$$[u_i] = b_i; \quad [\phi] = \Delta\phi; \quad [\psi] = \Delta\psi \tag{9}$$

where $[f]$ denotes the discontinuity of f across S. It is noted that the displacement jump is the traditional elastic dislocation, i.e., the Burgers vector. The electric potential jump $\Delta\phi$ corresponds to an electric dipole layer along the surface S (Barnett and Lothe, 1975), and hence is called the electric potential dislocation (Pak, 1990). $\Delta\psi$ is called the magnetic potential dislocation (Kirchner and Alshits, 1996). The strength of the extended dislocation is expressed by the extended Burgers vector $\mathbf{b} = [b_1, b_2, b_3, \Delta\phi, \Delta\psi]^T$. On the dislocation surface S, we assume that there is no force, no electric charge and no electric current. Thus the elastic traction, the normal components of the electric displacement and magnetic induction are continuous across the surface, i.e.

$$[\sigma_{ji}n_j] = 0; \quad [D_j n_j] = 0; \quad [B_j n_j] = 0 \tag{10}$$

The conditions Eqs. (9) and (10) on the dislocation surface S can be expressed by the extended components as

$$[u_J] = b_J; \quad [\sigma_{iJ}n_i] = 0; \quad J = 1 \sim 5 \tag{11}$$

For the problem of an extended dislocation loop in an anisotropic MEE medium, we further assume that the extended body force is zero ($f_J = 0$). Then, substituting Eq. (11) into Eq. (8), we find that the extended displacement field produced by an extended dislocation loop can be expressed as

$$u_M(\boldsymbol{y}) = \int_S C_{iJKl}(\boldsymbol{x})G_{KM,x_l}(\boldsymbol{y};\boldsymbol{x})b_J(\boldsymbol{x})n_i(\boldsymbol{x})dS(\boldsymbol{x}) \tag{12}$$

with S being the surface surrounded by the dislocation loop L.

The extended displacement gradient is

$$u_{M,p}(\boldsymbol{y}) = \int_S C_{iJKl}(\boldsymbol{x})G_{KM,x_l y_p}(\boldsymbol{y};\boldsymbol{x})b_J(\boldsymbol{x})n_i(\boldsymbol{x})dS(\boldsymbol{x}) \tag{13}$$

3.1. Line-integral solution along the dislocation loop

For an infinite homogeneous space, noticing that $G_{KM,x_l y_p}(\boldsymbol{y};\boldsymbol{x}) = -G_{KM,x_l x_p}(\boldsymbol{x}-\boldsymbol{y})$ and making use of the Stokes theorem, we can convert Eq. (13) into

$$u_{M,p}(\boldsymbol{y}) = -\int_S C_{iJKl}(\boldsymbol{x})G_{KM,x_l x_i}(\boldsymbol{y};\boldsymbol{x})b_J(\boldsymbol{x})n_p(\boldsymbol{x})dS(\boldsymbol{x}) - \varepsilon_{iph}\int_L C_{iJKl}(\boldsymbol{x})G_{KM,x_l}(\boldsymbol{y};\boldsymbol{x})b_M(\boldsymbol{x})v_h(\boldsymbol{x})dL(\boldsymbol{x}) \tag{14}$$

where ε_{ijk} is the permutation tensor and $\boldsymbol{v}$ is the unit tangent vector of the loop line along the boundary of the dislocation surface S. Assuming that the source point $\boldsymbol{y}$ is not on the dislocation surface, then the first term (integral on the surface of the dislocation) vanishes since the point-force Green's function satisfies the homogeneous equilibrium equation. Thus, the extended displacement gradient field is expressed as a line integral along the dislocation loop L of the dislocation surface

$$u_{M,p}(\boldsymbol{y}) = -\varepsilon_{iph}\int_L C_{iJKl}(\boldsymbol{x})G_{KM,x_l}(\boldsymbol{y};\boldsymbol{x})b_M(\boldsymbol{x})v_h(\boldsymbol{x})dL(\boldsymbol{x}) \tag{15}$$

Eq. (15) can be written in a compact form as

$$u_{I,j}(\boldsymbol{y}) = \int_L \beta_{jIh}(\boldsymbol{y};\boldsymbol{x})dL_h(\boldsymbol{x}) \tag{16a}$$

with

$$\beta_{jIh}(\boldsymbol{y};\boldsymbol{x}) = \varepsilon_{njh}b_M C_{nMKl}G_{KI,x_l}(\boldsymbol{x}-\boldsymbol{y}) \tag{16b}$$

The extended stress field produced by the dislocation can be expressed as

$$\sigma_{iJ}(\boldsymbol{y}) = \int_L S_{iJh}(\boldsymbol{y};\boldsymbol{x})dL_h(\boldsymbol{x}) \tag{17a}$$

with

$$S_{iJh}(\boldsymbol{y};\boldsymbol{x}) = C_{iJKl}\varepsilon_{nlh}b_M C_{nMPq}G_{KP,x_q}(\boldsymbol{x}-\boldsymbol{y}) \tag{17b}$$

The kernel $S_{iJh}(\boldsymbol{y};\boldsymbol{x})$ can be considered as the iJ-component of the extended stress at $\boldsymbol{y}$ produced by a line element of dislocation with extended Burgers vector $\mathbf{b}$ lying in the x_h-direction at $\boldsymbol{x}$, whilst $\beta_{iJh}(\boldsymbol{y};\boldsymbol{x})$ in Eq. (16) can be considered as the corresponding displacement gradient. By setting the appropriate coefficients to zero, the integral solutions (16) and (17) can be reduced to the corresponding solutions for the pure elasticity and piezoelectricity (Mura, 1987; Nowacki and Alshits, 2007) .

3.2. Analytical expressions of the fields produced by piecewise straight dislocation lines

The displacement gradient and stress fields produced by a dislocation loop can be obtained by direct numerical integration employing the line integration expressions. (16) and (17). Since the kernels, i.e., the generalized Green's functions (their derivatives), are involved in these integrals, which have no analytical solutions for the general anisotropic medium, methods based on the numerical evaluation of these integration expressions require substantial computation time. Thus it would be very appealing to obtain analytical integral expression due to dislocations,

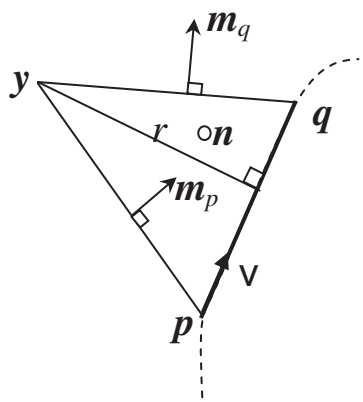

Fig. 1. Schematic of a straight-line segment ***pq*** of the dislocation where ***y*** is the field point of the dislocation, ***n*** is the normal of the triangle plane ***qpy***, pointing away from the paper.

even for some special dislocation lines, say a straight dislocation line. Furthermore, the solution for the straight dislocation segment is fundamental for any shape of dislocation loop, since an arbitrary dislocation loop can be approximated by summing a finite number of small straight dislocation lines (or the segments). We thus provide such an analytical integration below.

Substituting, first, the Green's function expression (A2) in Appendix A into Eq. (16), we have

$$u_{I,j}(\boldsymbol{y}) = \frac{-i}{(2\pi)^3}\varepsilon_{njh} b_M C_{nMKl} \int_L dL_h(\boldsymbol{x}) \int\int\int_{-\infty}^{\infty} \xi_l \times \frac{A_{Kl}(\boldsymbol{\xi})}{D(\boldsymbol{\xi})} e^{i(\boldsymbol{y}-\boldsymbol{x})\cdot\boldsymbol{\xi}} d\xi_1\xi_2\xi_3 \tag{18}$$

Now let us consider a general straight dislocation segment from point ***p*** to point ***q*** as shown in Fig. 1. Then, an arbitrary point ***x*** on it can be expressed by

$$\boldsymbol{x} = \boldsymbol{p} + t(\boldsymbol{q}-\boldsymbol{p}), \quad 0 \le t \le 1 \tag{19}$$

Substituting Eq. (19) into Eq. (18), the displacement gradient produced by this straight dislocation segment is reduced to

$$u_{I,j}(\boldsymbol{y}) = \frac{-i}{(2\pi)^3}\varepsilon_{njh} b_M C_{nMKl}(b_{h-a_h}) \int_0^1 dt \times \int\int\int_{-\infty}^{\infty} \xi_l \times \frac{A_{Kl}(\boldsymbol{\xi})}{D(\boldsymbol{\xi})} e^{i[\mathbf{y}-\mathbf{p}-t(\mathbf{q}-\mathbf{p})]\cdot\boldsymbol{\xi}} d\xi_1\xi_2\xi_3 \tag{20}$$

Following the integration procedure in elasticity (Willis, 1970; Mura, 1987), the gradient field produced by this straight dislocation segment is obtained as

$$u_{I,j}(\boldsymbol{y}) = \frac{1}{8\pi^2}\varepsilon_{njh} b_M C_{nMKl} v_h r^{-1}[I_{lKl}(\boldsymbol{m}_b,\boldsymbol{n}) - I_{lKl}(\boldsymbol{m}_a,\boldsymbol{n})] \tag{21a}$$

with

$$I_{lKl}(\boldsymbol{m},\boldsymbol{n}) = \int_0^{2\pi} d\phi \frac{(m_l\cos\phi + n_l\sin\phi)A_{Kl}(\boldsymbol{m}\cos\phi + \boldsymbol{n}\sin\phi)}{\cos\phi D(\boldsymbol{m}\cos\phi + \boldsymbol{n}\sin\phi)} \tag{21b}$$

In Eq. (21), ***v*** is again the unit tangent vector along the straight line with components $v_h = (q_h - p_h)/|\boldsymbol{q}-\boldsymbol{p}|$; r is the distance from the field point ***y*** to the straight line ***q – p***. Three unit vectors $\boldsymbol{m}_p$, $\boldsymbol{m}_q$ and ***n*** are introduced, as shown in Fig. 1, where $\boldsymbol{n} = \boldsymbol{v}\times(\boldsymbol{y}-\boldsymbol{p})/|\boldsymbol{v}\times(\boldsymbol{y}-\boldsymbol{p})|$ is normal to the plane containing points ***y***, ***p*** and ***q***; $\boldsymbol{m}_p$ is orthogonal to ***n*** and ***p – y***; and $\boldsymbol{m}_q$ is orthogonal to ***n*** and ***q – y***.

Compared with Eq. (16), it can be seen that the following expression

$$\frac{1}{8\pi^2} r^{-1}[I_{lKl}(\boldsymbol{m}_q,\boldsymbol{n}) - I_{lKl}(\boldsymbol{m}_p,\boldsymbol{n})]$$

corresponds to the term $G_{Kl,x_l}(\boldsymbol{x}-\boldsymbol{y})$ in Eq. (16b). Thus, this term can be considered as the derivative of the extended Green's function displacements produced by the straight dislocation segment.

For the special case of an infinite long straight dislocation, $\boldsymbol{m}_p = -\boldsymbol{m}_q$ with $\boldsymbol{m}_q$ being simply denoted by ***m***, which is further normal to the dislocation line. Then we have $I_{lKl}(\boldsymbol{m}_p,\boldsymbol{n}) = -I_{lKl}(\boldsymbol{m},\boldsymbol{n})$, and thus the displacement gradient field produced by the infinite straight dislocation is reduced to

$$u_{I,j}(\boldsymbol{y}) = \frac{1}{(2\pi)^2}\varepsilon_{njh} b_M C_{nMKl} v_h r^{-1} I_{lKl}(\boldsymbol{m},\boldsymbol{n}) \tag{22}$$

with $\boldsymbol{n} = \boldsymbol{v}\times\boldsymbol{m}$.

We point out that the analytical expression (21a) is for the derivative of the extended displacement field induced by a dislocation of straight-line segment. Thus this approach can only provide the extended strain and stresses fields analytically; the extended displacement field remains unsolvable analytically. Furthermore, the solution is for the straight-line segment dislocation, even though a general dislocation curve could be approximated by a finite number of piece-wise straight-line segments. The solution provided in the next section, however, can not only be applied to various curved segments of dislocation directly, but also provides analytical expressions for the extended displacement field.

3.3. Analytical expression of the fields produced by parametric dislocation curves

Dislocations are often complex in shapes, and thus parametric description of these curves has certain advantages (Ghoniem et al., 2000). However, the fields produced by these parametric dislocation loops are not easy to calculate, especially for anisotropic materials. If the fields produced by some useful parametric dislocation curves, such as elliptic arc and conic curves, can be analytically integrated out, it would provide us with great computational efficiency and accuracy, and thus makes dislocation dynamics simulation in an anisotropic material feasible.

We start from the surface integral expressions (12) and (13) of the dislocation field and assume that the dislocation surface is located on a flat plane. Thus, if the material properties are constants on the dislocation plane, we can write Eqs. (12) and (13) as

$$u_M(\boldsymbol{y}) = b_J n_i C_{ijKl} \int_S G_{KM,x_l}(\boldsymbol{y};\boldsymbol{x}) dS(\boldsymbol{x}) \tag{23}$$

$$u_{M,p}(\boldsymbol{y}) = b_J n_i C_{ijKl} \int_S G_{KM,x_l y_p}(\boldsymbol{y};\boldsymbol{x}) dS(\boldsymbol{x}) \tag{24}$$

From these equations it can be seen that, in order to find the dislocation-induced field, one needs to carry out the surface integration over the dislocation surface of the derivatives of the point-force Green's functions. We will then focus on these integrations. Substituting the Green's function solutions (A8) and (A9) in Appendix A, we have the surface integrations as

$$\int_S G(\boldsymbol{y};\boldsymbol{x})_{,x_l}\mathrm{d}S(x)=\begin{cases}\frac{-1}{2\pi^2}\int_0^\pi \bar{\boldsymbol{A}}[\int_S(\boldsymbol{G}_u^{(1)})_{,x_l}\mathrm{d}S(\boldsymbol{x})]\bar{\boldsymbol{A}}^T\mathrm{d}\theta, & x_3>y_3\\ \frac{1}{2\pi^2}\int_0^\pi \boldsymbol{A}[\int_S(\boldsymbol{G}_u^{(2)})_{,x_l}\mathrm{d}S(\boldsymbol{x})]\boldsymbol{A}^T\mathrm{d}\theta, & x_3<y_3\end{cases} \tag{25}$$

with

$$\begin{cases}\int_S(\boldsymbol{G}_u^{(1)})_{ij,x_l}\mathrm{d}S(\boldsymbol{x})=-\delta_{ij}h_l(\bar{p}_i)\int_S\frac{\mathrm{d}S(\boldsymbol{x})}{[\mathbf{h}(\theta,\bar{p}_i).(\mathbf{x}-\mathbf{y})]^2}, & x_3>y_3\\ \int_S(\boldsymbol{G}_u^{(2)})_{ij,x_l}\mathrm{d}S(\boldsymbol{x})=-\delta_{ij}h_l(p_i)\int_S\frac{\mathrm{d}S(\mathbf{x})}{[\mathbf{h}(\theta,p_i).(\mathbf{x}-\mathbf{y})]^2}, & x_3<y_3\end{cases} \tag{26}$$

$$\mathbf{h}(\theta,p_i)=[\cos\theta,\sin\theta,p_i]^T,\quad \mathbf{h}(\theta,\bar{p}_i)=[\cos\theta,\sin\theta,\bar{p}_i]^T \tag{27}$$

and

$$\int_S G_{,x_ly_p}(\boldsymbol{y};\boldsymbol{x})dS(\boldsymbol{x})=\begin{cases}\frac{-1}{2\pi^2}\int_0^\pi \bar{\boldsymbol{A}}[\int_S(\boldsymbol{G}_u^{(1)})_{,x_ly_p}\mathrm{d}S(\boldsymbol{x})]\bar{\boldsymbol{A}}^T\mathrm{d}\theta, & x_3>y_3\\ \frac{1}{2\pi^2}\int_0^\pi \boldsymbol{A}[\int_S(\boldsymbol{G}_u^{(2)})_{,x_ly_p}\mathrm{d}S(\boldsymbol{x})]\boldsymbol{A}^T\mathrm{d}\theta, & x_3<y_3\end{cases} \tag{28}$$

with

$$\begin{cases}\int_S(\boldsymbol{G}_u^{(1)})_{ij,x_ly_p}\mathrm{d}S(\boldsymbol{x})=-2\delta_{ij}h_l(\bar{p}_i)h_p(\bar{p}_i)\int_S\frac{\mathrm{d}S(\boldsymbol{x})}{[\mathbf{h}(\theta,\bar{p}_i)\cdot(\mathbf{x}-\mathbf{y})]^3}, & x_3>y_3\\ \int_S(\boldsymbol{G}_u^{(2)})_{ij,x_ly_p}\mathrm{d}S(\boldsymbol{x})=-2\delta_{ij}h_l(p_i)h_p(p_i)\int_S\frac{\mathrm{d}S(\boldsymbol{x})}{[\mathbf{h}(\theta,p_i)\cdot(\mathbf{x}-\mathbf{y})]^3}, & x_3<y_3\end{cases} \tag{29}$$

From Eqs. (26) and (29), it can be seen that the key problem is to carry out the following kind of integration over the dislocation loop surface:

$$F_n(\boldsymbol{y},\theta,p)=\int_S\frac{\mathrm{d}S(\boldsymbol{x})}{[\mathbf{h}(\theta,p)\cdot(\mathbf{x}-\mathbf{y})]^n}\quad n=2,3 \tag{30}$$

where p can be assigned to different eigenvalues, according to the requirements in Eqs. (26) and (29). In order to carry out the surface integration in Eq. (30) over a dislocation loop surface, we first transform the global coordinate system (O: x_1,x_2,x_3) to a local coordinate system ($\boldsymbol{x}_0$: ξ_1,ξ_2,ξ_3), with the base vectors ξ_1^0 and ξ_2^0 being on the dislocation plane, and ξ_3^0 normal to such a plane. Therefore, a point $\boldsymbol{x}$ on the dislocation plane is transformed to ξ by the coordinate transformation

$$[\boldsymbol{x}-\boldsymbol{x}_0]=[\mathbf{D}][\xi] \tag{31}$$

where $D_{ij}=\boldsymbol{x}_i^0\cdot\xi_j^0$ and $\boldsymbol{x}_0$ being the origin of the local coordinates. Then, the integration in Eq. (30) becomes

$$F_n(\boldsymbol{y},\theta,p)=\int_S\frac{\mathrm{d}\xi_1\mathrm{d}\xi_2}{[f_1(\boldsymbol{y},\theta)\xi_1+f_2(\boldsymbol{y},\theta)\xi_2+f_3(\boldsymbol{y},\theta)]^n}\quad n=2,3 \tag{32}$$

with

$$f_\alpha(\boldsymbol{y},\theta,p)=D_{k\alpha}h_k(\theta,p),\quad \alpha=1,2 \tag{33}$$

and $f_3(\boldsymbol{y},\theta,p)=(x_{0k}-y_k)h_k(\theta,p)$.

By introducing (Tan and Sun, 2006; Chu et al. 2012)

$$L_n(\xi_1,\xi_2)=\int_{-\infty}^{\xi_2}\frac{\mathrm{d}\xi_2}{(f_1\xi_1+f_2\xi_2+f_3)^n}\quad n=2,3 \tag{34}$$

one has

$$\frac{\partial L_n(\xi_1,\xi_2)}{\partial\xi_2}=\frac{1}{(f_1\xi_1+f_2\xi_2+f_3)^n}\quad n=2,3 \tag{35}$$

Substituting Eq. (34) to Eq. (32), one gets

$$F_n=\int_S\frac{\partial L_n(\xi_1,\xi_2)}{\partial\xi_2}\mathrm{d}\xi_1\mathrm{d}\xi_2=\int_L L_n(\xi_1,\xi_2)\mathrm{d}\xi_1\quad n=2,3 \tag{36}$$

Thus, the surface integral over the dislocation plane is transformed into the line integral along the dislocation loop line L.

By definition (33), L_n can be integrated analytically as

$$L_2(\xi_1,\xi_2)=-\frac{1}{f_2}\frac{1}{f_1\xi_1+f_2\xi_2+f_3},\quad L_3(\xi_1,\xi_2)=-\frac{1}{2f_2}\frac{1}{(f_1\xi_1+f_2\xi_2+f_3)^2} \tag{37}$$

Now, let us assume that the dislocation loop or dislocation segment can be described by some kind of parametric forms (Ghoniem et al., 2000), in the local (ξ_1,ξ_2)-plane, as

$$\xi(t)=N_i(t)\boldsymbol{q}_i \tag{38}$$

where $\boldsymbol{q}_i$ is a set of generalized coordinates, t is a parameter, and $N_i(t)$ are the shape functions.

Based on the parametric expression, Eq. (35) becomes

$$F_n=\int_l L_n(\xi_1,\xi_2)\mathrm{d}\xi_1=\int_{t_1}^{t_2}L_n[N_i(t)q_{i1},N_i(t)q_{i2}]N_{i,t}(t)q_{i1}\mathrm{d}t\quad n=2,3 \tag{39}$$

For some parametric curves of dislocations, one can obtain analytically the integration in Eq. (38). Presented below are the analytical results for two common dislocation segments, a straight line segment and an elliptic arc segment.

3.3.1. A straight line segment

For the special case of a straight line segment, in the local (ξ_1,ξ_2)-plane it can be described by

$$\xi(t)=(1-t)\boldsymbol{P}_1+t\boldsymbol{P}_2,\quad 0\le t\le 1 \tag{40}$$

where $\boldsymbol{P}_1$ and $\boldsymbol{P}_2$ are the position vectors of the start and end points of the straight line segment. Substituting Eq. (39) into (36) and then (38), the integration of (38) can be obtained as

$$F_2^{seg}=-\frac{1}{f_2}\frac{P_{21}-P_{11}}{f_1(P_{21}-P_{11})+f_2(P_{22}-P_{12})}\mathrm{In}\frac{f_1P_{21}+f_2P_{22}+f_3}{f_1P_{11}+f_2P_{12}+f_3} \tag{40a}$$

$$F_3^{seg}=\frac{1}{2f_2}\frac{P_{21}-P_{11}}{f_1(P_{21}-P_{11})+f_2(P_{22}-P_{12})}\left(\frac{1}{f_1P_{21}+f_2P_{22}+f_3}-\frac{1}{f_1P_{11}+f_2P_{12}+f_3}\right) \tag{40b}$$

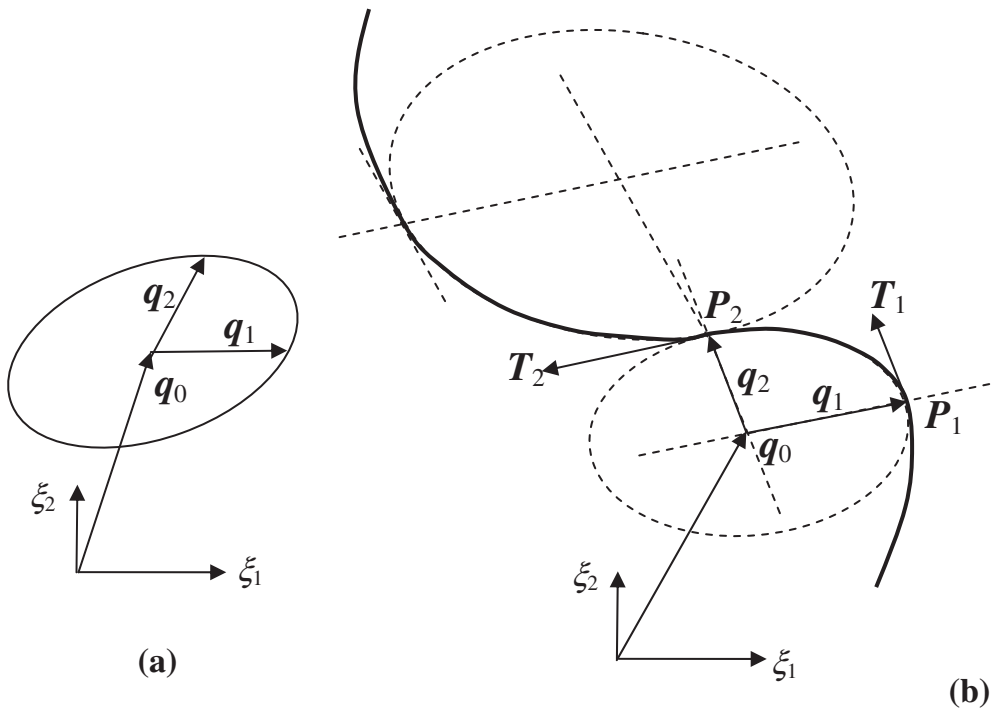

Fig. 2. (a) Schematic of an elliptic loop where $\boldsymbol{q}_0$ is the center vector of the ellipse, $\boldsymbol{q}_1$ the relative start vector at the parameter $t = 0$ (relative to the center $\boldsymbol{q}_0$), and $\boldsymbol{q}_2$ the relative vector at $t = \pi/2$. It is noted that the position vectors $\boldsymbol{q}_1$ and $\boldsymbol{q}_2$ are not necessarily normal to each other. (b) Schematic of representing a smooth dislocation curve segment via a couple of elliptic arcs with $t = 0 \sim \pi/2$.

3.3.2. An elliptic arc segment

For the case of a dislocation curve described by an elliptic arc segment, in the local (ξ_1, ξ_2)-plane, we first express the ellipse in terms of the parameter t as,

$$\xi(t) = \boldsymbol{q}_1 \cos t + \boldsymbol{q}_2 \sin t + \boldsymbol{q}_0, \quad -\pi \le t \le \pi \tag{41}$$

with $\boldsymbol{q}_0$, $\boldsymbol{q}_1$ and $\boldsymbol{q}_2$ being the vectors used to describe the ellipse, see Fig. 2(a).

Then, the denominator in Eq. (36) can be expressed as

$$\begin{aligned} f_1\xi_1 + f_2\xi_2 + f_3 &= f_\alpha q_{1\alpha} \cos t + f_\alpha q_{2\alpha} \sin t + f_\alpha q_{0\alpha} + f_3 \\ &= c_1 \cos t + c_2 \sin t + c_3 \end{aligned} \tag{42}$$

where summation is taken on the repeated index α from 1 to 2. One also notes that

$$\begin{aligned} \mathrm{d}\xi_1 &= (-q_{11} \sin t + q_{21} \cos t)\mathrm{d}t \\ &= (c_4 \cos t + c_5 \sin t)\mathrm{d}t \end{aligned} \tag{43}$$

Substituting Eqs. (42) and (43) into Eqs. (36) and (38), the integration of Eq. (38) along the elliptic arc $t_1 \le t \le t_2$ can be obtained as

$$\begin{aligned} F_2^{arc} &= -\frac{1}{f_2}\int_{t_1}^{t_2} \frac{c_4 \cos t + c_5 \sin t}{c_1 \cos t + c_2 \sin t + c_3}\mathrm{d}t \\ &= -\frac{1}{f_2}\frac{1}{c_1^2 + c_2^2}[(c_1c_4 + c_2c_5)(t - c_3I_1) + (c_2c_4 - c_1c_5) \\ &\quad \times \ln(c_1 \cos t + c_2 \sin t + c_3)]|_{t_1}^{t_2} \end{aligned} \tag{44a}$$

$$\begin{aligned} F_3^{arc} &= -\frac{1}{2f_2}\int_{t_1}^{t_2} \frac{c_4 \cos t + c_5 \sin t}{(c_1 \cos t + c_2 \sin t + c_3)^2}\mathrm{d}t \\ &= -\frac{1}{2f_2}\frac{1}{c_1^2 + c_2^2 - c_3^2}\left[(c_1c_4 + c_2c_5)I_1 \right. \\ &\quad \left. + \frac{c_1c_5 - c_2c_4 + c_3c_5 \cos t - c_3c_4 \sin t}{c_1 \cos t + c_2 \sin t + c_3}\right]\Bigg|_{t_1}^{t_2} \end{aligned} \tag{44b}$$

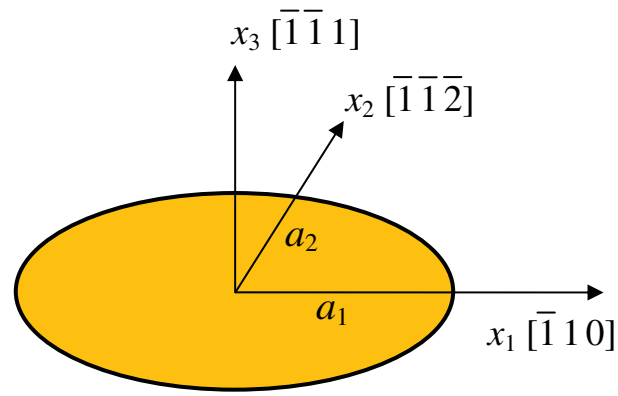

Fig. 3. Geometry of an elliptic dislocation loop in a cubic material which is located in the close-packed-$(\bar{1}\,\bar{1}\,1)$ plane. In the analysis, this close-packed plane is on the (x_1, x_2)-plane, and the major semi-axis length of the ellipse is a_1 along x_1-axis, and the minor semi-axis length is a_2 along x_2-axis.

where

$$I_1(t) = \frac{-2}{\sqrt{c_3^2 - c_1^2 - c_2^2}} \arctan \frac{(c_1 - c_3)\tan\frac{t}{2} - c_2}{\sqrt{c_3^2 - c_1^2 - c_2^2}}$$

The elliptic arc solution would be a powerful tool in describing and simulating the dislocation curve. Although the elliptic arc parameter range t can be chosen freely, for convenience, we will use only one quarter of the elliptic arc with $0 \le t \le \pi/2$ to describe a curved dislocation loop. Assume that we have a curved but smooth dislocation segment, with $\boldsymbol{P}_1$ and $\boldsymbol{P}_2$ being the position vectors of the start and end points of the curve, and $\boldsymbol{T}_1$ and $\boldsymbol{T}_2$ being the tangential vectors at these two points, see Fig. 2(b). In

Table 1a
Stress field ($\times 10^8$ Pa b/a_1) at point $(x_1,x_2, x_3)/a_1 = (1, 2, 3)$ due to the elliptic dislocation with $a_2/a_1 = 0.712$.

b	σ_{11}	σ_{22}	σ_{33}	σ_{23}	σ_{31}	σ_{12}
b [100]	−0.1463536	1.17260190	2.3282018	1.8072880	−0.47679743	0.6170828
Ref	−0.1464	1.1726	2.3282	1.8073	−0.4768	0.6171
Elastic	−0.14978	1.16418	2.32381	1.80504	−0.47658	0.61514
b[010]	−0.5924890	0.4148779	5.5483323	2.7604305	1.8072880	0.9336515
Ref	−0.5925	0.4149	5.5483	2.7604	1.8073	0.9337
Elastic	−0.58558	0.41347	5.53346	2.75277	1.80504	0.93437
b[001]	−0.9986909	2.6647172	1.5138506	5.5483323	2.3282018	1.9058421
Ref	−0.9987	2.6647	1.5138	5.5483	2.3282	1.9058
Elastic	−0.99046	2.65060	1.49739	5.53346	2.32381	1.9058

Ref: Results by Minagawa (2003).

Table 1b
Electric field ($\times 10^6$ b/a_1 $\times$V/m) at point $(x_1,x_2, x_3)/a_1 = (1,2, 3)$ due to the elliptic dislocation with $a_2/a_1 = 0.712$.

b	E_1	E_1 (Ref)	E_2	E_2 (Ref)	E_3	E_3 (Ref)
b[100]	0.7321277	0.7321	−3.1087848	−3.1088	1.0174471	1.0174
b[010]	−1.3759902	−1.3760	−7.9399963	−7.9400	4.9293209	4.9293
b[001]	−0.7766583	−0.7767	−14.0025322	−14.0030	7.2078685	7.2079

Ref: Results by Minagawa (2003), should be in unit 10^6V/m.

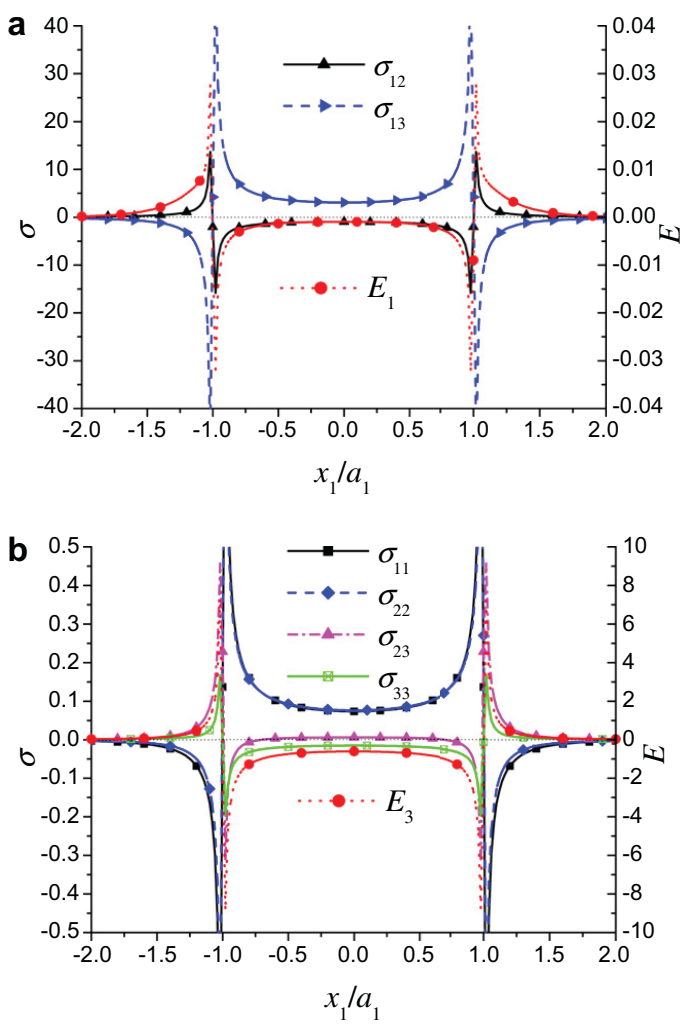

Fig. 4. (a). The induced stresses ($\times 10^{10} b/a_1$ Pa) and electric field ($\times 10^8 b/a_1$ V/m) along x_1-axis in the loop plane produced by an elliptic dislocation loop with Burgers vector **b** = $b(1,0, 0, 0, 0)$. (b). The induced stresses ($\times 10^{10}\Delta\phi/a_1$ Pa m/V) and electric field ($\times 10^8\Delta\phi/a_1$) along x_1-axis in the loop plane produced by an elliptic dislocation loop with Burgers vector **b** = $(0,0, 0, \Delta\phi,0)$.

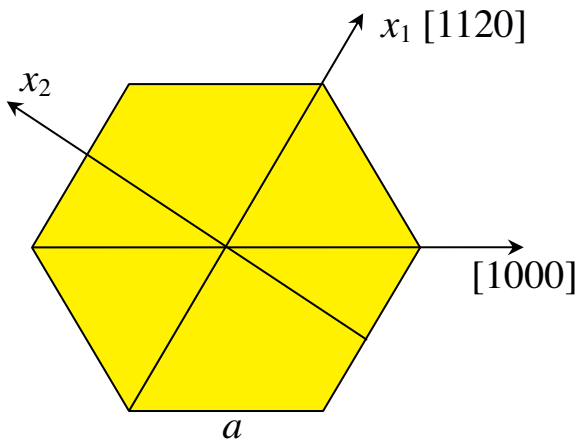

Fig. 5. Geometry of a hexagonal dislocation loop with side length a located in the global (x_1,x_2)-plane.

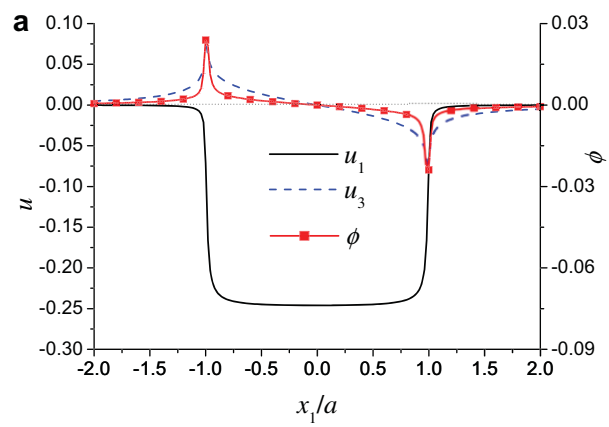

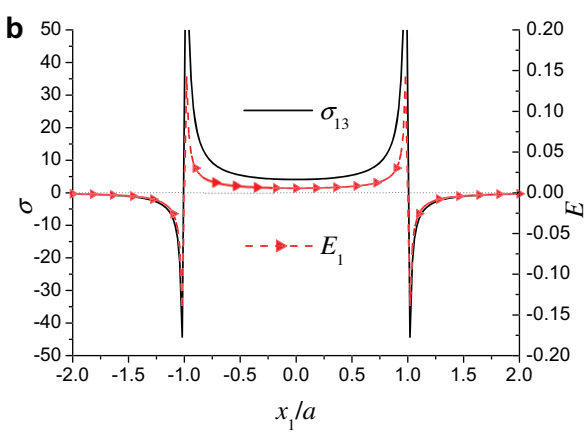

Fig. 6a,b. The fields along x_1-axis in the loop plane produced by a hexagonal dislocation loop with Burgers vector $\mathbf{b} = b(1,\ 0,\ 0,\ 0,\ 0)$: Displacements ($\times 2b$) and electric potential ($\times 2b\ 10^8$V/m) in (a), which are calculated on the plane $x_3 = 0.01a$; stresses ($\times 2b/a\ 10^{10}$Pa) and electric field ($\times 2b/a\ 10^8$V/m) in (b).

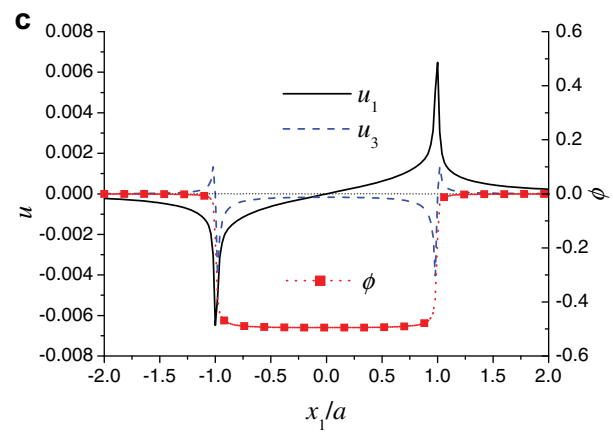

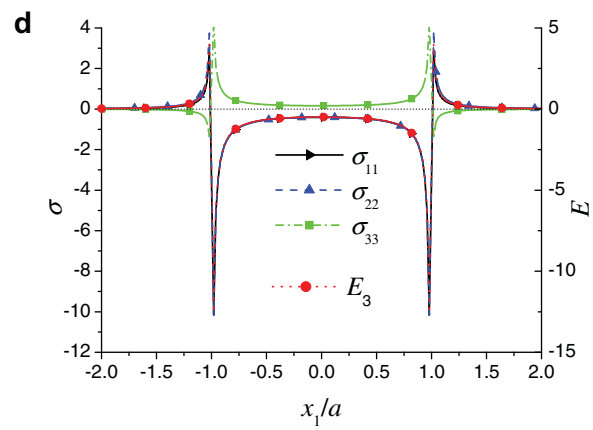

Fig. 6c,d. The fields along x_1-axis in the loop plane produced by a hexagonal dislocation loop with Burgers vector $\mathbf{b} = (0,0,\ 0,\ \Delta\phi,0)$: displacements ($\times\Delta\phi$/V m) and electric potential ($\times\Delta\phi\ 10^8$) in (c), which are calculated on the plane x_3=0.01a; stresses ($\times\Delta\phi/a\ 10^{10}$ Pa m/V) and electric field ($\times\Delta\phi/a\ 10^8$) in (d).

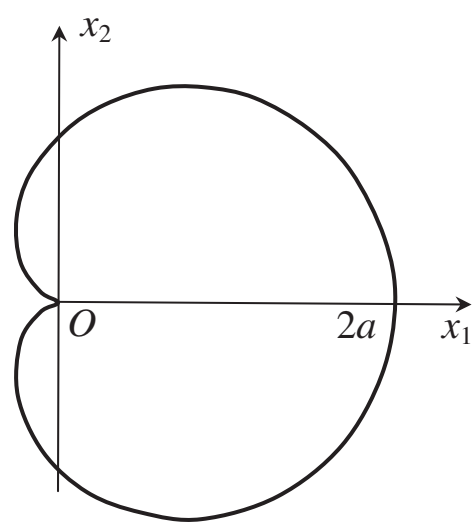

Fig. 7. Schematic of a cardioid dislocation loop lying on the global (x_1,x_2)-plane.

order to describe the curve by a quarter elliptic arc, we first draw at point $\boldsymbol{P}_1$ a straight line which is parallel to $\boldsymbol{T}_2$. At point $\boldsymbol{P}_2$ we draw another line parallel to $\boldsymbol{T}_1$. The intersection point of the two lines is the center $\boldsymbol{q}_0$ of the ellipse. We set $\boldsymbol{q}_1 = \boldsymbol{P}_1 - \boldsymbol{q}_0$, $\boldsymbol{q}_2 = \boldsymbol{P}_2 - \boldsymbol{q}_0$, and then we can use the quarter elliptic arc $\xi(t) = \boldsymbol{q}_1 \cos t + \boldsymbol{q}_2 \sin t + \boldsymbol{q}_0 (0 \le t \le \pi/2)$ to represent the dislocation curve. In this way, the elliptic arc and the dislocation curve will

Table 2a
Displacement field ($\times 10^{-3}$ b), electric potential ϕ ($\times 10^{6}$ b V/m) and magnetic potential ψ ($\times 10^{3}$ b A/m) at point $(x_1,x_2,\ x_3)/a = (1,2,3)$ due to a cardioid dislocation with $\mathbf{b} = b(1,0,0,0,0)$.

Methods	Segments	u_1	u_2	u_3	ϕ	ψ
Straight line Eq. (39)	20	−5.76616	−0.97513	−2.20788	−0.77808	−1.05305
	200	−5.9818016	−0.9659598	−2.2061220	−0.7786773	−1.0547746
	1000	−5.9839352	−0.9658665	−2.2060976	−0.7786805	−1.0547878
Parametric elliptic arc Eq. (42)	20	−5.95498	−0.96739	−2.20691	−0.77878	−1.05479
	200	−5.9831489	−0.9658766	−2.2061003	−0.7786802	−1.0547864
	1000	−5.9812148	−0.9658632	−2.2060967	−0.7786806	−1.0547883

Table 2b
Stress field ($\times 10^{8}$ Pa b/a) at point $(x_1,x_2,\ x_3)/a = (1,\ 2,\ 3)$ due to a cardioid dislocation with $\mathbf{b} = b(1,\ 0,\ 0,\ 0,\ 0)$.

Methods	Segments	σ_{11}	σ_{22}	σ_{33}	σ_{23}	σ_{31}	σ_{12}
Straight line Eqs. (21) or (40)	20	−0.40754	0.49500	1.60037	0.95275	−4.36251	−1.72935
	200	−0.4020991	0.4858708	1.6039867	0.9424102	−4.4809286	−1.7596709
	1000	−0.4020444	0.4857799	1.6040166	0.9423052	−4.4820791	−1.7599577
Parametric elliptic arc Eq. (44)	20	−0.40287	0.48716	1.60390	0.94397	−4.46634	−1.75600
	200	−0.4020503	0.4857898	1.6040134	0.9423166	−4.4819548	−1.7599267
	1000	−0.4020424	0.4857767	1.6040177	0.9423015	−4.4821201	−1.7599679
Num. Integ. Eq. (17)	160 Gauss points	−0.4020421	0.4857762	1.6040178	0.9423008	−4.4821270	−1.7599696

Table 2c
Electric field E ($\times 10^{6}$ $b/a \times$ V/m) and magnetic field H ($\times 10^{3}$ b/a $\times$A/m) at point $(x_1,x_2,\ x_3)/a = (1,\ 2,\ 3)$ due to a cardioid dislocation with b= $b(1,\ 0,\ 0,\ 0,\ 0)$.

Methods	Segments	E_1	E_2	E_3	H_1	H_2	H_3
Straight line Eqs. (21) and (40)	20	4.18427	−0.70696	−0.25522	5.51235	−1.20986	−0.16849
	200	4.3105460	−0.6991563	−0.2593337	5.6762831	−1.1955773	−0.1772010
	1000	4.3117781	−0.6990771	−0.2593729	5.6778790	−1.1954326	−0.1772852
Parametric elliptic arcs Eq. (44)	20	4.29493	−0.70032	−0.25885	5.65601	−1.19769	−0.17608
	200	4.3116450	−0.6990857	−0.2593687	5.6777066	−1.1954482	−0.1772761
	1000	4.3118220	−0.6990742	−0.2593743	5.6779359	−1.1954274	−0.1772882
Line Integral Eq. (17)	160 Gauss points	4.3118294	−0.6990738	−−0.2593745	5.6779454	−1.1954265	−0.1772887

Table 3a
Elastic displacements ($\times 10^{-3}$ m), electric potential ϕ ($\times 10^{6}$ V), and magnetic potential ψ ($\times 10^{3}$ A) at point $(x_1,x_2,\ x_3)/a = (1,\ 2,\ 3)$ due to a cardioid dislocation with $\mathbf{b} = b(0,\ 1,\ 0,\ 0,\ 0)$, $b(0,\ 0,\ 1,\ 0,\ 0)$, $(0,\ 0,\ 0,\ \Delta\phi,0)$, and $(0,\ 0,\ 0,\ 0,\ \Delta\psi)$. The extended displacements in the second, third, fourth, and fifth rows are further normalized, respectively, by b/m, b/m, $\Delta\phi$/V, and $\Delta\psi$/A.

b	u_1	u_2	u_3	ϕ	ψ
$b(0,1,\ 0,\ 0,\ 0)$	−0.9660745	−17.5405689	−24.7623214	−8.3047326	−10.8032097
$b(0,\ 0,\ 1,\ 0,\ 0)$	−1.6339115	−18.1852151	−43.4819849	−15.9888860	−22.3323875
$(0,\ 0,\ 0,\ \Delta\phi,0)$	−0.5389647	−5.8311939	−12.3458347	−262.4805324	0.8063630
$(0,\ 0,\ 0,\ 0,\ \Delta\psi)$	−26.2826030	−308.4147293	−294.2080133	−415.7494406	−96621.18859

Table 3b
Stress components ($\times 10^{8}$ Pa) at point $(x_1,x_2,\ x_3)/a = (1,\ 2,\ 3)$ due to a cardioid dislocation with $\mathbf{b} = b(0,1,\ 0,\ 0,\ 0)$, $b(0,\ 0,\ 1,\ 0,\ 0)$, $(0,\ 0,\ 0,\ \Delta\phi,0)$, and $(0,\ 0,\ 0,\ 0,\ \Delta\psi)$. The results in the second, third, fourth, and fifth rows are further normalized, respectively, by b/a, b/a, $\Delta\phi/a \times m$/V, and $\Delta\psi/a \times m$/A.

b	σ_{11}	σ_{22}	σ_{33}	σ_{23}	σ_{31}	σ_{12}
$b(0,1,\ 0,\ 0,\ 0)$	−0.7573445	2.5277051	16.9367799	6.4102858	0.9423008	0.3898098
$b(0,0,\ 1,\ 0,\ 0)$	−4.6591357	7.4104605	14.4744986	16.9367799	1.6040178	1.0454428
$(0,\ 0,0,\ \Delta\phi,0)$	−4.2609289	0.9324061	10.7339201	12.20010	1.1394653	0.4506775
$(0,\ 0,\ 0,\ 0,\ \Delta\psi)$	−124.1184048	−24.6916913	191.9138012	194.3473273	16.7180673	8.0629309

have the same tangent at the start and end points. Making use of this kind of elliptic arcs continuously, the continuity of the tangent of the dislocation curve will be kept, and the loop will be smooth.

We mention that analytical integration of the dislocation solution can also be obtained for many other types of curves in parametric forms, one of the other examples is the conic curve, for which an analytical integration can be also found.

Table 3c
Electric field ($\times 10^6$ V/m) and magnetic field H ($\times 10^3$ A/m) at point $(x_1,x_2,x_3)/a = (1,2,3)$ due to a cardioid dislocation with $\mathbf{b} = b(0,1,0,0,0)$, $b(0,0,1,0,v)$, $(0,0,0,\Delta\phi,0)$, and $(0,0,0,0,\Delta\psi)$. The results in the second, third, fourth, and fifth rows are further normalized, respectively, by b/a, b/a, $\Delta\phi/a \times$ m/V, and $\Delta\psi/a \times$ m/A.

b	E_1	E_2	E_3	H_1	H_2	H_3
$b(0,1,0,0,0)$	−0.7004319	−3.5785148	−2.0687722	−1.1966802	−7.7730422	−0.2751957
$b(0,0,1,0,0)$	−1.5073361	−15.6291039	−0.7333146	−2.6132255	−27.0040043	2.0950967
$(0,0,0,\Delta\phi,0)$	−10.8287132	−119.8065533	−91.9075071	−0.8703930	−8.5800570	5.5001202
$(0,0,0,0,\Delta\psi)$	−17.7295045	−201.0272276	−133.467933	−1302.36062	−15347.9542	−52725.0705

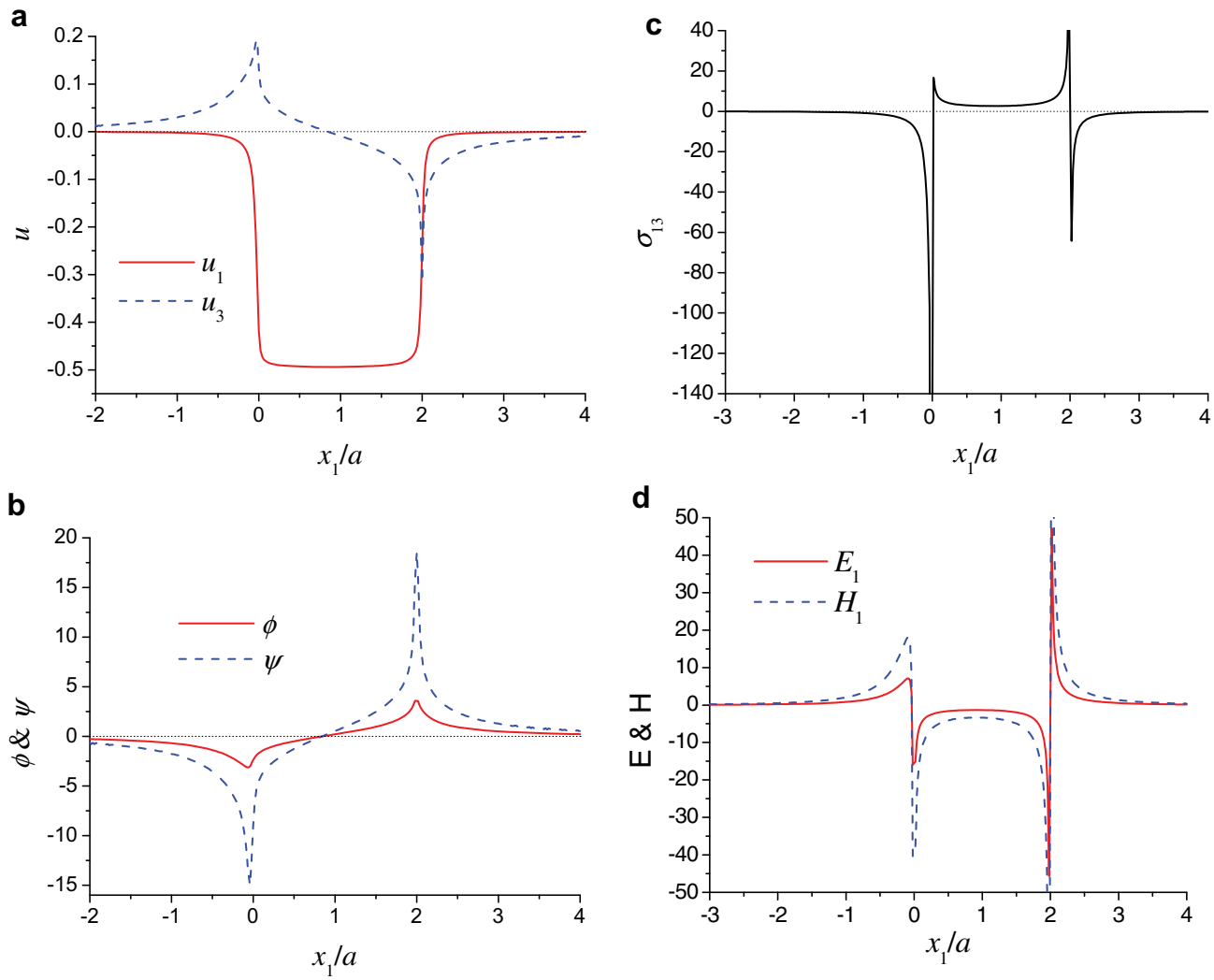

Fig. 8. The fields along x_1-axis in the loop plane produced by a cardioid dislocation with Burgers vector $\mathbf{b} = b(1,0,\ 0,\ 0,\ 0)$: Elastic displacements ($\times b$) in (a), and electric potential ($\times b$ 10^8V/m) and magnetic potential ($\times b$ 10^4A/m) in (b), stress ($\times b/a$ 10^{10} Pa) in (c), electric fields ($\times b/a$ 10^8 V/m) and magnetic fields ($\times b/a$ 10^4 A/m) in (d). (a) and (b) are on the plane $x_3 = 0.01a$.

4. Numerical examples

4.1. Case 1: An elliptic dislocation loop in a piezoelectric space made of cubic GaAs

We consider a dislocation loop in an infinite piezoelectric space made of gallium arsenide (GaAs) crystal. This cubic crystal GaAs has an fcc structure and its material constants are listed in Appendix B (Minagawa and Shintani, 1985).

We assume that the elliptic dislocation loop lies on the close-packed $(\bar{1}\,\bar{1}\,1)$ - plane, and we attach the x_1-, x_2- and x_3-axes of the global coordinates along, respectively, the $[\bar{1}\,1\,0]$-, $[\bar{1}\,\bar{1}\,\bar{2}]$- and $[\bar{1}\,\bar{1}\,1]$-directions of the crystal. The major axis of the elliptical loop is along x_1-axis with semi-axis length of a_1, and its minor axis is along x_2-axis with semi-axis length of a_2 (see Fig. 3). In our calculation, the ratio a_2/a_1 is fixed at 0.712, and a_1 is used as the unit length of the coordinates.

As a validation, we first calculate the stress and electric fields at the field point $(x_1, x_2, x_3) = (1,2,3)a_1$ produced by this elliptic loop with its Burgers vector (the elastic dislocation part) along different directions. It shows that the

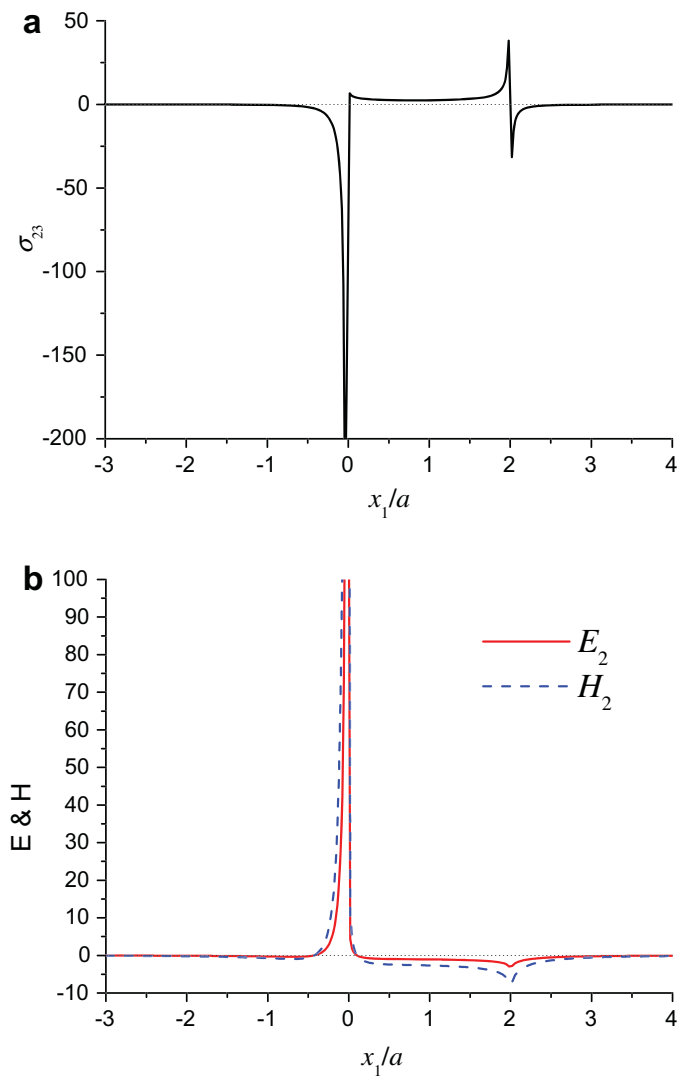

Fig. 9. The fields along x_1-axis in the loop plane produced by a cardioid dislocation with Burgers vector $\mathbf{b} = b(0,1,\ 0,\ 0,0)$: Stress ($\times 10^{10}$ Pa) in (a); and electric field ($\times 10^8$ V/m) and magnetic field ($\times 10^4$ A/m) in (b). Quantities are further normalized by b/a.

results by the direct numerical line integration of Eq. (17) (using 160 Gauss quadrature points) and those by the analytical line segment method of Eq. (21) (using 1000 straight line segments) are the same, and that both further agree well with those by Minagawa (2003), see Table 1. When the electric effect is ignored, the pure elastic results are also given which are exactly the same as those by the surface integration method (Han and Ghoniem, 2005).

The fields (nonzero components) on the loop plane along x_1-axis produced by the elliptic dislocation loop with $\mathbf{b} = b(1,0,\ 0,\ 0,\ 0)$ and $(0,\ 0,\ 0,\ \Delta\phi,0)$ are shown in Fig. 4a and b, respectively. In Fig. 4a, the stresses are normalized by (10^{10} Pa $\times\ b/a_1$), and the electric fields are normalized by (10^8 V/m $\times\ b/a_1$). In Fig. 4b, the stresses are normalized by (10^{10} Pa $\times\ \Delta\phi/a_1 \times$ m/V), and the electric fields are normalized by ($10^8 \times \Delta\phi/a_1$).

From Fig. 4a and b, it is observed that the induced stress and electric fields by either an elastic or an electric dislocation are singular near the dislocation loop. Under the elastic dislocation $\mathbf{b} = b(1,0,\ 0,\ 0,\ 0)$, the induced electric field **E** will be mainly along the dislocation direction **b**. For this case, the induced nonzero electric component is E_1, which has a similar shape as σ_{12} and is in the range of 10^7 V/m $\times\ b/a_1$. The electric dislocation $\Delta\phi$ would induce mainly normal stresses and the electric field normal to the dislocation plane. For this case, the induced nonzero electric component is E_3, which has a very similar variation as σ_{33}, and is in the range of $10^9 \times \Delta\phi/a_1$.

4.2. Case 2: A hexagonal dislocation loop in a piezoelectric space made of hexagonal AlN

We now consider a hexagonal dislocation loop which lies on the {0001} plane of an hcp-packed crystal made of piezoelectric aluminum nitrides (AlN) (Fig. 5). This hexagonal loop is located in the global (x_1,x_2)-plane with a side length a. The material properties of AlN are listed in Appendix B (Singh, 1993; Pan and Yang, 2003).

Since the hexagonal dislocation is made of six straight line segments, both straight line dislocation solutions, i.e.

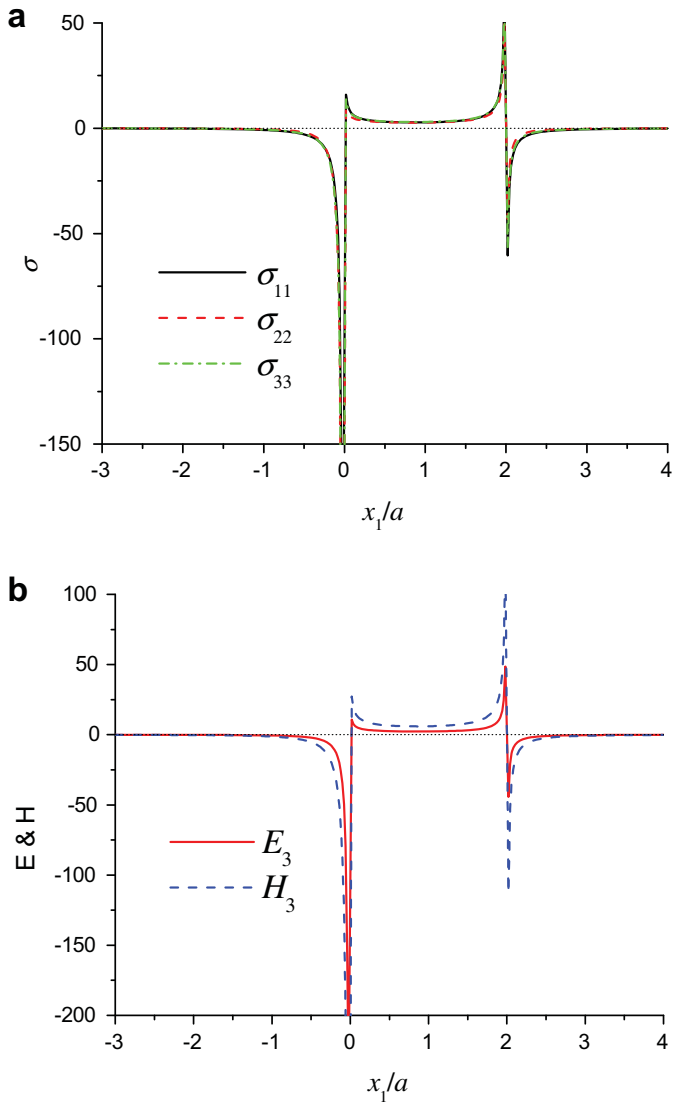

Fig. 10. The fields along x_1-axis in the loop plane produced by a cardioid dislocation with Burgers vector $\mathbf{b} = b(0,0,\ 1,\ 0,\ 0)$: Stresses ($\times 10^{10}$ Pa) in (a); and electric field ($\times 10^{8}$ V/m) and magnetic field ($\times 10^{4}$ A/m) in (b). Quantities are further normalized by b/a.

Eqs. (21) and (40) can be applied. It was shown that both solutions (for the induced extended strain and stress fields) predict exactly the same results. However, Eq. (40) includes also the analytical solutions of the extended displacement. Thus, the results presented below are based on the solution of Eq. (40). It needs to mention that, though the two methods give the same results for a closed dislocation loop, but for a separate finite dislocation segment, the results by the two methods are generally different. When a dislocation line tends to an infinite straight dislocation line, the two methods give the same results again. Since different segment solutions may come from different solutions of a closed loop, they are only physically meaningful for a closed loop or an infinite long dislocation.

Figs. 6a–6d show the displacement and stress fields produced by the hexagonal dislocation loop on the {0001}-plane. While Figs. 6a and 6b are those due to the elastic dislocation along the crystal direction $\langle 11\bar{2}0\rangle$ or along x_1-axis, Figs. 6c and 6d are those due to an electric potential dislocation $\Delta\phi$. From these figures, we can see the strong coupling effect between elastic and electric near the dislocation line, i.e. an elastic dislocation can induce strong electric field, and vice versa. In general, for the given hexagonal material with the special orientation of the dislocation loop, an elastic dislocation can induce an electric field **E** in the same direction of the elastic Burgers vector **b**, and an electric potential dislocation can induce mainly normal stress fields as well as an electric field **E** normal to the dislocation plane.

4.3. Case 3: A cardioid dislocation loop in an MEE space

The shapes of dislocations in materials usually are complex than regular ones. Cardioid-shaped dislocations are common in materials when dislocations are pinned by defects during their expansion or multiplication process. Fig. 7 shows a cardioid dislocation loop on the plane $x_3 = 0$ in a $BaTiO_3$–$CoFe_2O_4$ MEE composite. While the MEE material is based on the 50% $BaTiO_3$ and 50% $CoFe_2O_4$

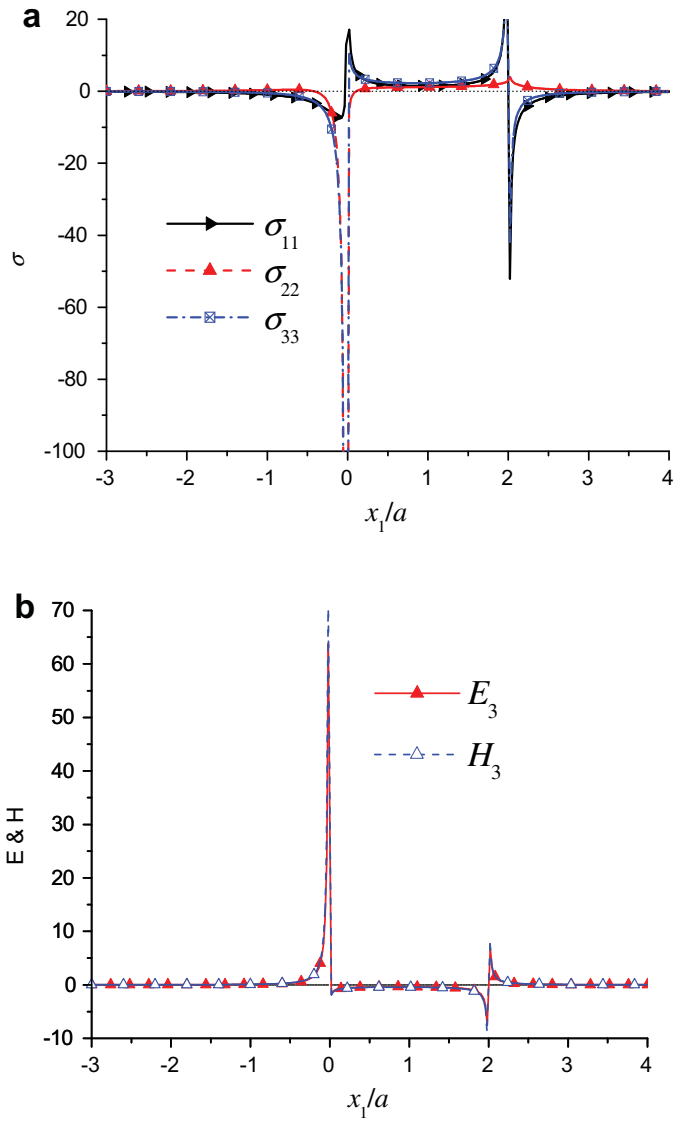

Fig. 11. The fields along x_1-axis in the loop plane produced by a cardioid dislocation loop with Burgers vector $\mathbf{b} = (0, 0, 0, \Delta\phi, 0)$: stresses ($\times 10^{10}$ Pa) in (a); and electric field ($\times 10^{8}$ V/m) and magnetic field ($\times 10^{6}$ A/m) in (b). Quantities are further normalized by $\Delta\phi/a \times$ m/V.

with its properties listed in Appendix B, the parametric expression of the loop is described by

$$x_1(t) = a\cos(t)[1 + \cos(t)],$$
$$x_2(t) = a\sin(t)[1 + \cos(t)], \quad 0 \le t \le 2\pi$$

with a being the shape parameter of the cardioid.

We first calculate the fields at point $(x_1, x_2, x_3) = (1, 2, 3)a$. For $\mathbf{b} = b(1, 0, 0, 0, 0)$, the field results are listed in Table 2, using different methods, including the direct numerical line integration method Eq. (17) (using 160 Gauss points), two straight line segment methods Eqs. (21) and (40), and the parametric elliptic arc method Eq. (44). From this tables, we can see that the results calculated by the four methods agree well with each other if enough Gauss integration points and dislocation line segments are used. When 20, 200 and 1000 parametric elliptic arcs are used, the results will be accurate to 3, 5 and 7 digital numbers, respectively. When 20, 200 and 1000 straight segments are used, the results will be accurate to 2, 4 and 6 digital numbers, which are less accurate than those by the elliptic arc methods. Thus, if a dislocation loop has less curvature, the straight line segment methods Eqs. (21) or (40) are suitable, with the latter further giving the extended displacement field with the same accuracy. When a dislocation loop has a complex curved shape, then the parametric curve method, such as the analytical elliptic arc method, is more suitable. The direct numerical line integration method Eq. (17) can be used, if the shape of a dislocation loop can be mathematically described well, which is usually not easier for a moving dislocation in dislocation dynamics simulation. Thus, for a dislocation loop with complex shape and with rapid changing shape, a parametric curve description and analysis has more advantage. Furthermore, the parametric method can also predict the extended displacement fields if needed.

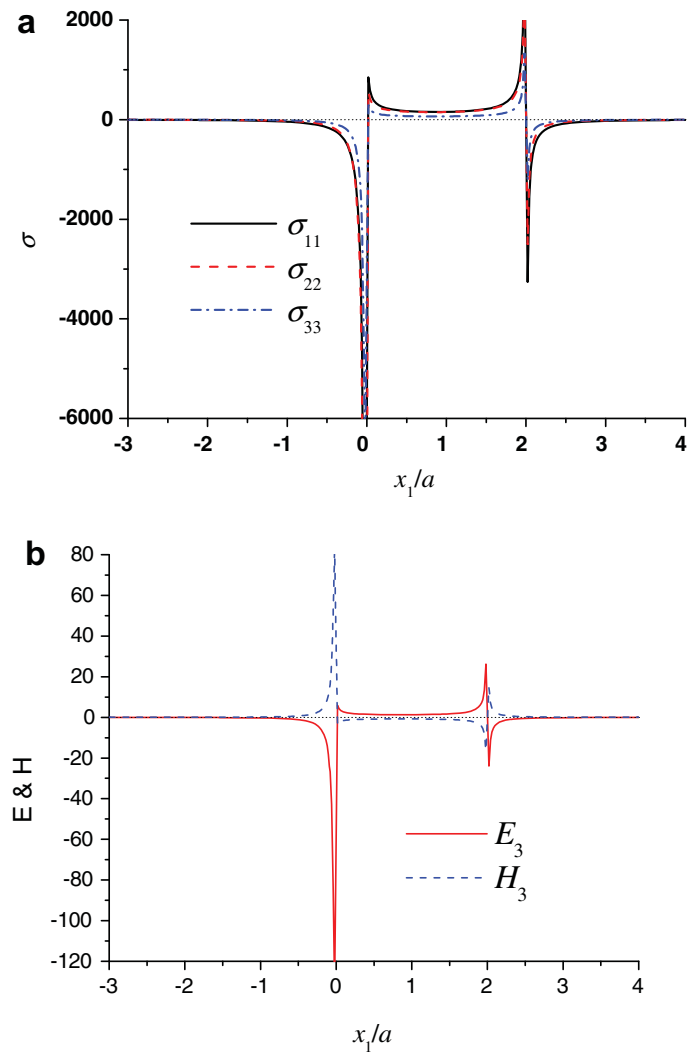

Fig. 12. The fields along x_1-axis in the loop plane produced by a cardioid dislocation loop with Burgers vector **b** = (0, 0, 0, 0, $\Delta\psi$): stresses ($\times 10^{10}$ Pa) in (a); AMD electric field ($\times 10^{10}$ V/m) and magnetic field ($\times 10^{10}$ A/m) in (b). Quantities are further normalized by $\Delta\psi/a \times m$/A.

For the dislocation with different kinds of Burger's vectors, including the electric and magnetic ones, the field results at point $(x_1,x_2,x_3) = (1,2,3)a$ are given in Table 3. From this tables, we can observe clearly the coupling effect among the elastic, electric and magnetic fields.

The fields along x_1-axis are shown in Figs. 8–12, from which we can see the strong field coupling effect near the dislocation loop line. From these figures, we observe that besides the induced stress fields, a displacement dislocation **b** can also induce the electric and magnetic fields due to the coupling effect. Furthermore, these induced fields are singular near the dislocation line, with **E** and **H** mainly along the direction of the dislocation vector **b**. On the other hand, an electric potential dislocation $\Delta\phi$ or magnetic potential dislocation $\Delta\psi$ can induce the electric field **E** and the magnetic fields **H**, which are singular near the dislocation core and are normal to the dislocation plane, and the singular stress fields (mainly normal components) near the dislocation core due to the coupling effects.

5. Conclusions and discussion

First we extend the anisotropic dislocations formulae in elasticity to those in magneto-electro-elastic materials, including a line integration expression and an analytical solution of the straight line dislocation. Then we develop a new line integration solution of dislocation fields and derive the analytical expressions for some useful parametric dislocation curves, such as elliptic arc, straight line, et al. The piezoelectric, piezomagnetic, and purely anisotropic elastic solutions are all included by the present solutions by setting the appropriate material coefficients to zero. The present solution is an extension to the anisotropic elastic theory of dislocations (Hirth and Lothe, 1982).

Different numerical and analytical solutions are compared in this paper. For a dislocation loop with less curvature, straight line segment methods are suitable; for a complex curved dislocation loop, an integrable parametric dislocation solution is more appealing. For a dislocation loop with a complex and rapid changing shape, a

parametric curve description and the corresponding analytical integration expression are more advantageous than the straight-line segment solution. Furthermore, the extended displacement fields can be also obtained via the parametric dislocation solution method.

Three typical dislocation loops are chosen as examples, including an elliptic loop in piezoelectric GaAs, a hexagonal loop in piezoelectric AlN, and a cardioid loop in $BaTiO_3$–$CoFe_2O_4$ magneto-electro-elastic materials. These examples show clearly the coupling effect among the elastic, electric and magneto fields. For instance, besides the induced stress fields, an elastic dislocation can also induce the electric and magnetic fields due to the coupling effect, and also these induced fields are singular near the dislocation line.

For piezoelectric and magneto-electro-elastic materials, we only considered the coupling fields induced by dislocations. Some dislocation related problems, such as dislocation charge phenomena, dislocation scattering effect to electron or photon, dislocation movement, etc., are yet to be investigated. Due to the elastic strain and coupling effect, a dislocation could induce polarization electric field and polarization charges. In addition, due to the defects in crystal structure of dislocation core and the singularity in coupling field, external charged impurities are often accumulated on the dislocation core, and the dislocation may become a negatively or positively charged dislocation. In order to neutralize the dislocation core charges, a charged dislocation is likely to be screened by charges of opposite sign in its surrounding area. The movement of charged and screened dislocations need more energy and therefore will be more difficult to move. Consequently, these materials are more likely to be brittle than plastic. Moreover, the charged dislocation can induce the scattering effect when electrons or photons pass through the core area. There are many related problems need further investigation in these materials.

Acknowledgements

The authors are grateful for the support from the National Natural Science Foundation of China under Grant Nos. 11272052 and 11172273 and China Scholarship Council.

Appendix A. Extended Green's functions and their derivatives

The extended point-force Green's functions and their derivatives in a generalized anisotropic MEE infinite space can be obtained by the Fourier transform method. For instance, based on the three-dimensional Fourier transformation, we have (Han, 2009)

$$G_{KM}(\boldsymbol{x}-\boldsymbol{y}) = \frac{1}{(2\pi)^3}\iiint_{-\infty}^{\infty}\frac{A_{KM}(\xi)}{D(\xi)}\mathrm{e}^{-\mathrm{i}(\boldsymbol{x}-\boldsymbol{y})\cdot\xi}\mathrm{d}\xi_1\xi_2\xi_3 \tag{A1}$$

$$G_{KM,x_l}(\boldsymbol{x}-\boldsymbol{y}) = \frac{-i}{(2\pi)^3}\iiint_{-\infty}^{\infty}\frac{A_{KM}(\xi)}{D(\xi)}\mathrm{e}^{-i(\boldsymbol{x}-\boldsymbol{y})\cdot\xi}\mathrm{d}\xi_1\xi_2\xi_3 \tag{A2}$$

where $A_{KM}(\xi)$ and $D(\xi)$ are, respectively, the adjoint matrix and determinant of $C_{ijKl}\xi_i\xi_l$.

Making use of the delta function property and carrying out the infinite integral, the Green's functions can be expressed as (Han, 2009)

$$G_{KM}(\boldsymbol{x}-\boldsymbol{y}) = \frac{1}{8\pi^2|\boldsymbol{x}-\boldsymbol{y}|}\oint_{C_\xi}\frac{A_{KM}(\xi)}{D(\xi)}\mathrm{d}\Omega \tag{A3}$$

The integral is now taken around the unit circle C_ξ on the plane normal to $\boldsymbol{x}$–$\boldsymbol{y}$.

The first derivative of the Green's functions can be expressed as

$$G_{KM,i}(\boldsymbol{x}-\boldsymbol{y}) = \frac{1}{8\pi^2|\boldsymbol{x}-\boldsymbol{y}|^2}\oint_{C_\xi}\{-x_i(\xi\xi)^{-1}_{KM} + \xi_i[(\boldsymbol{x}\xi)_{LN} + (\xi\mathbf{x})_{LN}](\xi\xi)^{-1}_{KL}(\xi\xi)^{-1}_{NM}\}\mathrm{d}\Omega \tag{A4}$$

with the notion $(\boldsymbol{AB})_{JK} = C_{iJKl}A_iA_l$ being used.

The Green's functions and their derivatives in a homogeneous 3D full space have the following symmetric properties

$$\begin{aligned} &G_{KM}(\boldsymbol{x};\boldsymbol{x}') = G_{KM}(\boldsymbol{x}-\boldsymbol{x}') = G_{MK}(\boldsymbol{x}-\boldsymbol{x}') = G_{KM}(\boldsymbol{x}'-\boldsymbol{x}),\\ &G_{KM,i}(\boldsymbol{x}-\boldsymbol{x}') = -G_{KM,i}(\boldsymbol{x}'-\boldsymbol{x}) = -G_{KM,i'}(\boldsymbol{x}-\boldsymbol{x}') \end{aligned} \tag{A5}$$

It is noted that the line-integral in Eqs. (A3) and (A4) can be evaluated by a numerical integral method, or by the Cauchy's residue theorem.

The extended Green's functions can also be solved via the two-dimensional Fourier transformation and the extended Stroh eigenequation method (Pan, 2002) as

$$\boldsymbol{G}(\boldsymbol{y};\boldsymbol{x}) = \begin{cases} -\frac{1}{2\pi^2}\int_0^\pi \bar{\boldsymbol{A}}\boldsymbol{G}_u^{(1)}\bar{\boldsymbol{A}}^T\mathrm{d}\theta, & x_3 > y_3\\ +\frac{1}{2\pi^2}\int_0^\pi \boldsymbol{A}\boldsymbol{G}_u^{(2)}\boldsymbol{A}^T\mathrm{d}\theta, & x_3 < y_3 \end{cases} \tag{A6}$$

where

$$\begin{aligned} &(\mathbf{G}_u^{(1)})_{IJ} = \frac{\delta_{IJ}}{\mathbf{h}(\theta,\bar{p}_I)\cdot(\mathbf{x}-\mathbf{y})};\quad (\mathbf{G}_u^{(2)})_{IJ} = \frac{\delta_{IJ}}{\mathbf{h}(\theta,p_I)\cdot(\mathbf{x}-\mathbf{y})}\\ &\mathbf{h}(\theta,p) = [\cos\theta,\sin\theta,p]^T;\mathbf{A} = [a_1,a_2,a_3,a_4,a_5] \end{aligned} \tag{A7}$$

and p_i, and a_i (i = 1–5) are the eigenvalues and the associated eigenvectors of the extended eigenequation:

$$[\mathbf{Q} + p(\mathbf{R}+\mathbf{R}^T) + p^2\mathbf{T}]\boldsymbol{a} = 0 \tag{A8}$$

where

$$\begin{aligned} &Q_{JK} = C_{iJKs}n_in_s,\quad R_{JK} = C_{iJK3}n_i,\\ &T_{JK} = C_{3JK3},\quad \boldsymbol{n} = [\cos\theta,\sin\theta,0]^T \end{aligned} \tag{A9}$$

and the eigenvalues and eigenvectors are selected such that

$$\mathrm{Im}(p_i) > 0,\quad p_{i+5} = \bar{p}_i,\ \bar{\boldsymbol{a}}_{i+5} = \bar{\boldsymbol{a}}_i,\quad (i = 1\sim 5) \tag{A10}$$

The derivatives of the extended Green's functions are

$$G(\boldsymbol{y};\boldsymbol{x})_{,x_l} = \begin{cases} \frac{-1}{2\pi^2}\int_0^\pi \bar{\boldsymbol{A}}(\mathbf{G}_u^{(1)})_{,x_l}\bar{\boldsymbol{A}}^T\mathrm{d}\theta, & x_3 > y_3\\ \frac{1}{2\pi^2}\int_0^\pi \boldsymbol{A}(\mathbf{G}_u^{(2)})_{,x_l}\boldsymbol{A}^T\mathrm{d}\theta, & x_3 < y_3 \end{cases} \tag{A11}$$

with

$$(\boldsymbol{G}_u^{(1)})_{ij,x_l} = \frac{-\delta_{ij} h_l(\bar{p}_i)}{[\mathbf{h}(\bar{p}_i)\cdot(\mathbf{x}-\mathbf{y})]^2}; \quad (\boldsymbol{G}_u^{(2)})_{ij,x_l} = \frac{-\delta_{ij} h_l(p_i)}{[\mathbf{h}(p_i)\cdot(\mathbf{x}-\mathbf{y})]^2} \tag{A12}$$

The second derivatives of the Green's functions are

$$\boldsymbol{G}(\boldsymbol{y};\boldsymbol{x})_{,x_l y_p} = \begin{cases} \frac{-1}{2\pi^2}\int_0^\pi \bar{\boldsymbol{A}}(\boldsymbol{G}_u^{(1)})_{,x_l y_p}\bar{\boldsymbol{A}}^T \mathrm{d}\theta, & x_3 > y_3 \\ \frac{1}{2\pi^2}\int_0^\pi \boldsymbol{A}(\boldsymbol{G}_u^{(2)})_{,x_l y_p}\mathbf{A}^T \mathrm{d}\theta, & x_3 < y_3 \end{cases} \tag{A13}$$

with

$$\begin{aligned} (\boldsymbol{G}_u^{(1)})_{ij,x_l y_p} &= \frac{-2\delta_{ij} h_l(\theta,\bar{p}_i) h_p(\theta,\bar{p}_i)}{[\mathbf{h}(\theta,\bar{p}_i)\cdot(\mathbf{x}-\mathbf{y})]^3} \\ (\boldsymbol{G}_u^{(2)})_{ij,x_l y_p} &= \frac{-2\delta_{ij} h_l(\theta,p_i) h_p(\theta,p_i)}{[\mathbf{h}(\theta,p_i)\cdot(\mathbf{x}-\mathbf{y})]^3} \end{aligned} \tag{A14}$$

Appendix B. Material properties

Elastic constants C_{ij} are in GPa ($\times 10^9$ N/m^2), piezoelectric constants e_{ij} in C/m^2, piezomagnetic constants q_{ij} in N/Am, dielectric constant (or permittivity) ε_{ij} in 10^{-9} F/m (or 10^{-9} C/(Vm) or 10^{-9} C^2/Nm^2), magnetic constants μ_{ij} in 10^{-4} H/m (or in 10^{-4} Ns^2/C^2).

(1) Piezoelectric (cubic) crystal properties of GaAs

C_{11}	C_{12}	C_{44}	$e_{14} = e_{25} = e_{36}$	$\varepsilon_{11} = \varepsilon_{22} = \varepsilon_{33}$
118.1	53.2	59.4	−0.16	0.1108

(1) Piezoelectric (transversely isotropic) crystal properties of AlN

C_{11}	C_{12}	C_{13}	C_{33}	C_{44}
396	137	108	373	116
$e_{31} = e_{32}$	e_{33}	$e_{24} = e_{15}$	$\varepsilon_{11} = \varepsilon_{22}$	ε_{33}
−0.58	1.55	−0.48	0.0797	0.0974

(1) 50%MEE $BaTiO_3$–$CoFe_2O_4$ composite properties

C_{11}	C_{12}	C_{13}	C_{33}	C_{44}
225	125	124	216	44
$e_{31} = e_{32}$	e_{33}	$e_{24} = e_{15}$	$\varepsilon_{11} = \varepsilon_{22}$	ε_{33}
−2.2	9.3	5.8	5.64	6.35
$q_{31} = q_{32}$	q_{33}	$q_{24} = q_{15}$	$\mu_{11} = \mu_{22}$	μ_{33}
290.2	350	275	2.97	0.835

References

Alpay, S.P., Misirlioglu, I.B., Nagarajan, V., Ramesh, R., 2004. Can interface dislocations degrade ferroelectric properties? Appl. Phys. Lett. 85, 2044–2046.

Barnett, D.M., Lothe, J., 1975. Dislocations and line charges in anisotropic piezoelectric insulators. Phys. Status Solidi B 67, 105–111.

Belabbas, I., Mimitrakopulos, G., Kioseoglou, J., Bere, A., Chen, J., Komninou, Ph., Ruterana, P., Nouet, G., 2006. Energetics of the 30° Shockley partial dislocation in wurtzite GaN. Superlattices Microstruct. 40, 458–463.

Chen, B.J., Xiao, Z.M., Liew, K.M., 2004. A screw dislocation interacting with a finite crack in a piezoelectric medium. Int. J. Eng. Sci. 42, 1325–1345.

Chu, H.J., Pan, E., Han, X., Wang, J., Beyerlein, I.J., 2012. Elastic fields of dislocation loops in three-dimensional anisotropic bimaterials. J. Mech. Phys. Solids 60, 418–431.

Ghoniem, N.M., Tong, S.-H., Sun, L.Z., 2000. Parametric dislocation dynamics: a thermodynamics-based approach to investigations of mesoscopic plastic deformation. Phys. Rev. B 61, 927–931.

Han, X., Ghoniem, N.M., 2005. Stress field and interaction forces of dislocations in anisotropic multilayer thin films. Philos. Mag. 85, 1205–1225.

Han, X., 2009. High-order derivatives of Green's functions in magneto-electro-elastic materials. Int. J. Solids Struct. 46, 3405–3411.

Hirth, J.P., Lothe, J., 1982. Theory of Dislocations. Wiley, New York.

Hao, R.J., Liu, J.X., 2006. Interaction of a screw dislocation with a semi-infinite interfacial crack in a magneto-electro-elastic bi-material. Mech. Res. Commun. 33, 415–424.

Hu, S.Y., Li, Y.L., Chen, L.Q., 2003. Effect of interfacial dislocations on ferroelectric phase stability and domain morphology in a thin film – a phase-field model. J. Appl. Phys. 94, 2542–2547.

Kirchner, H.O.K., Alshits, V.I., 1996. Elastically anisotropic angularly inhomogeneous media II. The Greens function for piezoelectric piezomagnetic magnetoelectric anisotropic media. Philos. Mag. 74, 861–885.

Lee, Jui-Mu, Ma, Chien-Ching, 2010. Image singularities of planar magnetoelectroelastic bimaterials for generalized line forces and edge dislocations. Eur. J. Mech. A/Solids 29, 420–439.

Li, S., Gupta, A., 2004. Peierls stress of a screw dislocation in a piezoelectric medium. Appl. Phys. Lett. 85, 2211–2213.

Liu, J.X., Du, S.Y., Wang, B., 1999. A screw dislocation interacting with a piezoelectric bimaterial interface. Mech. Res. Commun. 26, 415–420.

Ma, C.C., Lee, J.M., 2007. Image forces of screw dislocations in a magnetoelectroelastic layered half-plane. J. Appl. Phys. 101, 123513.

Minagawa, S., Shintani, K., 1985. Dislocation dynamics in anisotropic piezoelectric crystals. Philos. Mag. A 51, 277–285.

Minagawa, S., 2003. On the stress and electric field produced by dislocations in anisotropic piezoelectric crystals with special attention to the stress function. Mech. Mater. 35, 453–461.

Mura, T., 1987. Micromechanics of Defects in Solids. Martinus Nijhoff Publishers, Dordrecht.

Nowacki, J.P., Alshits, V.I., 2007. Dislocation fields in piezoelectrics. In: Nabarro, F.R.N., Hirth, J.P. (Eds.), Dislocations in Solids. Elsevier B.V., Chapter 72.

Pak, Y.E., 1990. Force on a piezoelectric screw dislocation. ASME J. Appl. Mech. 57, 863–869.

Pan, E., 2002. Three-dimensional Green's functions in anisotropic magneto-electro-elastic bimaterials. Journal of Applied Mathematics and Physics (ZAMP) 53, 815–838.

Pan, E., Yang, B., 2003. Elastic and piezoelectric fields in a substrate AlN due to a buried quantum dot. J. Appl. Phys. 93, 2435–2439.

Shi, C., Asbeck, P.M., Yu, E.T., 1999. Piezoelectric polarization associated with dislocations in wurtzite GaN. Appl. Phys. Lett. 74, 573–575.

Singh, J., 1993. Physics of Semiconductors and Their Heterostructures. McGraw-Hill, Inc., New York.

Soh, A.K., Liu, J.X., Lee, K.L., Fang, D.N., 2005. Moving dislocations in general anisotropic piezoelectric solids. Phys. Status Solidi B 242, 842–853.

Suo, Z., Kuo, C.-M., Barnett, D.M., Willis, J.R., 1992. Fracture mechanics for piezoelectric ceramics. J. Mech. Phys. Solids 40, 739–765.

Tan, E.H., Sun, L.Z., 2006. Stress field due to a dislocation loop in a heterogeneous thin film-substrate system, Modelling Simul. Mater. Sci. Eng. 14, 993–1013.

Wang, X., Sudak, L.J., 2007. A piezoelectric screw dislocation interacting with an imperfect piezoelectric bimaterial interface. Int. J. Solids Struct. 44, 3344–3358.

Willis, J.R., 1970. Stress fields produced by dislocations in anistropic media. Philos. Mag. 21, 931–940.

Zhang, T.Y., Zhao, M.H., Tong, P., 2002. Fracture of piezoelectric ceramics. Adv. Appl. Mech. 38, 147–289.

Zheng, Y., Wang, B., Woo, C.H., 2006. Simulation of interface dislocations effect on polarization distribution of ferroelectric thin films. Appl. Phys. Lett. 88, 092903.